

# Topographic Distribution and Progression of Soft Drusen Volume in Age-Related Macular Degeneration Implicate Neurobiology of Fovea

Andreas Pollreisz,<sup>1</sup> Gregor S. Reiter,<sup>1</sup> Hrvoje Bogunovic,<sup>1</sup> Lukas Baumann,<sup>2</sup> Astrid Jakob,<sup>1</sup> Ferdinand G. Schlanitz,<sup>1</sup> Stefan Sacu,<sup>1</sup> Cynthia Owsley,<sup>3</sup> Kenneth R. Sloan,<sup>3</sup> Christine A. Curcio,<sup>3</sup> and Ursula Schmidt-Erfurth<sup>1</sup>

<sup>1</sup>Department of Ophthalmology and Optometry, Medical University Vienna, Vienna, Austria

<sup>2</sup>Center for Medical Statistics, Informatics and Intelligent Systems, Medical University Vienna, Vienna, Austria

<sup>3</sup>Department of Ophthalmology and Visual Sciences, University of Alabama at Birmingham, Birmingham, Alabama, United States

Correspondence: Christine A. Curcio, Department of Ophthalmology and Visual Sciences; University of Alabama at Birmingham, 700 south 18th Street, Suite 601, Birmingham, AL 35294, USA; [christinecurcio@uabmc.edu](mailto:christinecurcio@uabmc.edu).

CAC and USE contributed equally to this work and share senior authorship.

**Received:** September 15, 2020

**Accepted:** December 1, 2020

**Published:** February 19, 2021

Citation: Pollreisz A, Reiter GS, Bogunovic H, et al. Topographic distribution and progression of soft drusen volume in age-related macular degeneration implicate neurobiology of fovea. *Invest Ophthalmol Vis Sci.* 2021;62(2):26. <https://doi.org/10.1167/iovs.62.2.26>

**PURPOSE.** To refine estimates of macular soft drusen abundance in eyes with age-related macular degeneration (AMD) and evaluate hypotheses about drusen biogenesis, we investigated topographic distribution and growth rates of drusen by optical coherence tomography (OCT). We compared results to retinal features with similar topographies (cone density and macular pigment) in healthy eyes.

**METHODS.** In a prospective study, distribution and growth rates of soft drusen in eyes with AMD were identified by human observers in OCT volumes and analyzed with computer-assistance. Published histologic data for macular cone densities ( $n = 12$  eyes) and in vivo macular pigment optical density (MPOD) measurements in older adults with unremarkable maculae ( $n = 31$ ; 62 paired eyes, averaged) were revisited. All values were normalized to Early Treatment Diabetic Retinopathy Study (ETDRS) subfield areas.

**RESULTS.** Sixty-two eyes of 44 patients were imaged for periods up to 78 months. Soft drusen volume per unit volume at baseline is 24.6-fold and 2.3-fold higher in the central ETDRS subfield than in outer and inner rings, respectively, and grows most prominently there. Corresponding ratios (central versus inner and central versus outer) for cone density in donor eyes is 13.3-fold and 5.1-fold and for MPOD, 24.6 and 23.9-fold, and 3.6 and 3.6-fold.

**CONCLUSIONS.** Normalized soft drusen volume in AMD eyes as assessed by OCT is  $\geq 20$ -fold higher in central ETDRS subfields than in outer rings, paralleling MPOD distribution in healthy eyes. Data on drusen volume support this metric for AMD risk assessment and clinical trial outcome measure. Alignment of different data modalities support the ETDRS grid for standardizing retinal topography in mechanistic studies of drusen biogenesis.

**Keywords:** age-related macular degeneration, AMD, Bruch's membrane, drusen, computational image analysis, OCT, optical coherence tomography, retinal pigment epithelium, soft drusen, fovea, cone photoreceptors, Müller glia, macular pigment

Age-related macular degeneration (AMD) causes vision loss worldwide and involves dysfunction of choriocapillaris, retinal pigment epithelium (RPE), photoreceptors with reactive gliosis, and driven by extracellular deposits between outer retinal cells and the circulation.<sup>1</sup> Current means to prevent progression to advanced AMD help just some patients.<sup>2</sup> Understanding the biology of population-level risk factors may inspire new approaches.

The largest and best documented intraocular risk factor for AMD progression is the abundance of drusen. These extracellular deposits between the RPE basal lamina and the inner collagenous layer of Bruch's membrane are dome-shaped, lipid-rich, and often continuous with a thin layer of the same material (basal linear deposit).<sup>3,4</sup> Druse-associated

progression risk is remarkably concentrated in the central macula, as specified by the central subfield and inner ring of the Early Treatment of Diabetic Retinopathy Study (ETDRS) grading grid in population-based observation studies using color fundus photography (CFP).<sup>5,6</sup>

Recent findings suggest that drusen reflect the activity of relatively functional cells (retina and RPE) and a dysfunctional vascular barrier (Bruch's membrane-choriocapillaris). These findings include Bruch's membrane lipid composition,<sup>7,8</sup> a cell culture model of deposit formation,<sup>9</sup> and a timeline of druse dynamism from clinical imaging.<sup>10,11</sup> Here, we explore the idea that the central concentration of drusen-related risk has a cellular basis in the healthy neurosensory retina by measuring drusen abundance in reference to reti-

nal candidate mechanisms. The human macula contains an area of cone photoreceptors only, with a central bouquet of very densely packed cells. By histology, cone density peaks at approximately 150,000/mm<sup>2</sup> of the retinal surface and decreases nearly symmetrically in all directions to 10% of these values by 1 mm eccentricity. In contrast, rods appear at approximately 175  $\mu\text{m}$  eccentricity and crest in an elliptical ring at 3 to 5 mm, encircling the optic nerve head.<sup>12</sup> In precisely these latter locations, subretinal drusenoid deposits (SDD; also known as reticular pseudodrusen) are apparent by imaging and histology in early and intermediate AMD eyes,<sup>13–15</sup> and also conferring risk for atrophy.<sup>16</sup> Because cones and rods have parallel physiologies adapted evolutionarily for different light levels, response speed, and neural circuitry, the discovery of SDD raised the possibility that drusen in central macula are related to densely packed cones, their support system, or both.<sup>17–19</sup> Limited histologic data indicate that soft drusen localize almost exclusively to the macula.<sup>20</sup>

Other cells that may be as numerous in the fovea as cones are the Müller glia, interleaved between them.<sup>21,22</sup> Recent research in glio-degenerative disease supports Müller glia as major reservoirs of macular pigment<sup>23</sup> (i.e. the xanthophyll carotenoids lutein and zeaxanthin). These yellow pigments peak sharply in the foveal center<sup>24</sup> and extend laterally into the two plexiform layers. Macular pigment and by inference, Müller glia, is quantifiable as macular pigment optical density (MPOD) using dual wavelength autofluorescence imaging.<sup>24,25</sup> This technology utilizes autofluorescence emission signal elicited from RPE by blue and green excitation lights. Intensities at fixation, where blue light is blocked by pigment, are compared with intensities at an eccentric reference point where pigment has dropped to near zero.

Optical coherence tomography (OCT) anchors multimodal retinal imaging and has revealed new aspects of AMD pathogenesis through detailed cross-sectional anatomy followed over time in vivo. Recently developed algorithms make it possible to quantify drusen load using macular OCT volume scans<sup>26–32</sup> with good repeatability and reproducibility compared to manual segmentation.<sup>29,33,34</sup> Whereas OCT<sup>35</sup> and histology<sup>36</sup> indicate that soft drusen are the most common type in the macula, hard and cuticular drusen are also visible in OCT scans<sup>37</sup> and may be captured by automated detection schema, along with RPE elevations due to other causes.<sup>4,38</sup>

In this prospective observational study, we analyzed the distribution of soft drusen that were identified in OCT volumes by human observers with computer-assistance. We investigated growth rates of soft drusen in follow-up periods of up to 78 months. To compare these findings with retinal cells, we comprehensively remapped published macular cone densities in whole mounts of human donor retinas,<sup>12,39</sup> and we re-plotted MPOD signal from dual wavelength autofluorescence imaging in older adults with normal maculae. The use of the ETDRS grid for all measures allowed direct topographic comparison of drusen abundance, drusen growth, cone density, and MPOD across these disparate samples.

## METHODS

This prospective and observational study adhered to the Declaration of Helsinki and Good Clinical Practice (GCP) guidelines. After approval by the Ethics Committee of the Medical University of Vienna and giving written informed consent, 44 patients with early and intermediate AMD were

included based on the clinical classification published by Ferris and associates.<sup>30</sup> Our study cohort is derived from a well-characterized study population with detailed medical history.<sup>11</sup> Patients are recruited from private practices of comprehensive ophthalmologists and thus represent an overall earlier stage of disease than typically seen at a tertiary referral center. Exclusion criteria were late AMD, defined as choroidal neovascularization or complete RPE and outer retinal atrophy, following the recent consensus published by Sadda and associates.<sup>31</sup> Patients were examined in a three-monthly interval, including best-corrected visual acuity (BCVA), complete ophthalmologic examination, including funduscopy, infra-red and blue light fundus autofluorescence images, and spectral domain OCT (SD-OCT; all Spectralis HRA + OCT; Heidelberg Engineering, Heidelberg, Germany) on each visit. Eye drops containing 0.5% tropicamide and 2.5% phenylephrine were administered for pupil dilation after the BCVA examination. Each patient was advised to take supplements<sup>32</sup> and reminded at every visit.

## SD-OCT Imaging and Drusen Analysis

All volume scans for this study were acquired with a Spectralis HRA + OCT (Heidelberg Engineering) using a resolution of 1024  $\times$  97 (A-scans  $\times$  B-scans) in a 6  $\times$  6 mm area. The OCT volume was centered on the fovea at the baseline visit and the follow-up mode in the software was used to re-acquire scans thereafter. Soft drusen were determined by two trained and experienced human readers (G.S.R. and A.J.) based on published distinctions between soft and hard drusen.<sup>3,40</sup> Hard drusen are defined as sub-RPE deposits with < 63  $\mu\text{m}$  in diameter and distinct borders at the level of Bruch's membrane.<sup>2</sup> Medium drusen are defined as 63 to 125  $\mu\text{m}$  in size. Large soft drusen were defined as dome shaped sub-RPE deposits with a horizontal diameter > 125  $\mu\text{m}$  and indistinct borders (Fig. 1).

Soft drusen were marked by human readers on all exported and applicable B-scans with software assistance using the in-house developed annotation tool Optimus (version 3.6; Medical University Vienna, Vienna, Austria). Three-dimensional (3D) retinal layer segmentation of a volumetric OCT scan, outlining the RPE and Bruch's membrane boundaries, was performed using the graph-based Iowa Reference Algorithm (Retinal Image Analysis Laboratory, Iowa Institute for Biomedical Imaging, Iowa City, IA, USA)<sup>18,33,34</sup> with a modified, relaxed smoothness constraint of RPE layer to account for drusen-related undulations. Human expert readers (G.S.R. and A.J.) double-checked segmentation lines from the algorithm in a randomly selected sample corresponding to 5% ( $n = 25$  volume scans) of the total dataset. To further reduce potential erroneous data points, outliers as determined by statistical analysis were additionally checked by expert readers for misaligned reference lines and adjusted if needed. Soft drusen was then identified as a contiguous segmented 3D region in-between RPE and Bruch's membrane that contained a marker from the human readers. Having soft drusen segmented in 3D allowed calculation of soft drusen volume, maximum height, and en face area, equivalent to a footprint.

Drusen volume, area, and maximum height were calculated for three fovea-centered zones based on subfields of the ETDRS grid. These include a central 1-mm-diameter disk, as well as inner and outer rings (internal-external radii of 0.5–1.5 mm and 1.5–3 mm, respectively).<sup>41</sup> The areas in mm<sup>2</sup> of these 3 regions are 0.79, 6.28, and 21.21, respectively.

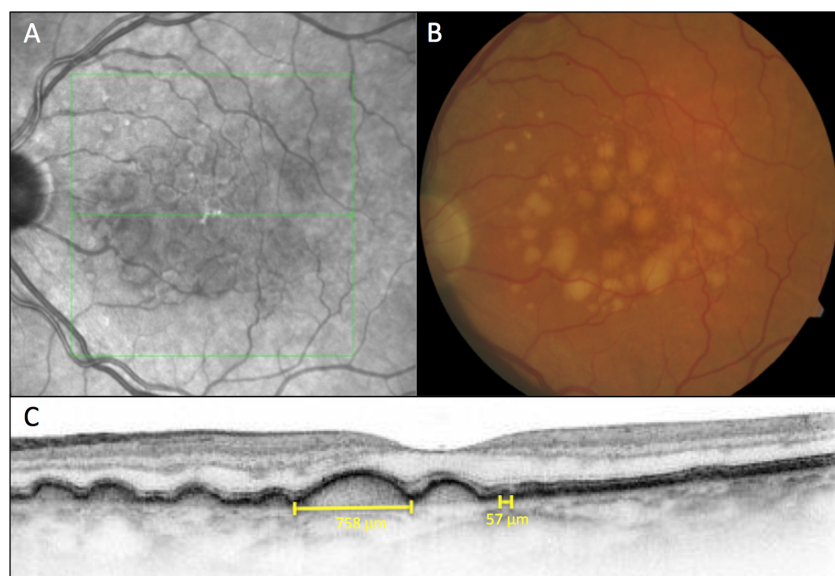


**FIGURE 1.** Large soft drusen are defined on SD-OCT B-scans as sub-RPE deposits with a horizontal diameter greater than 125  $\mu\text{m}$  and indistinct borders, while hard drusen are defined as sub-RPE deposits with less than 63  $\mu\text{m}$  in size and distinct borders at the level of Bruch's membrane. A near-infrared reflectance image (A) shows the level of the B-scan in panel C. A color fundus photograph (B) shows many typical soft drusen. An example of a soft druse with the maximum horizontal extent of 758  $\mu\text{m}$  and of a small hard druse with a horizontal extension of 57  $\mu\text{m}$  is indicated in panel (C).

After processing all scans, results for soft drusen volume, soft drusen area, and maximum soft drusen height within the central disk, inner ring, and outer ring were exported in tabular form. To quantify the spatial distribution of drusen as a function of eccentricity from the fovea, mean drusen height was computed along a circle, which, in practice with digital images, is a very thin annulus.

### Statistics

Due to the differing areas of the ETDRS subfields, soft drusen volume was normalized as soft drusen volume in nanoliter (nL) per  $\text{mm}^2$  of retinal surface. Soft drusen area was normalized as  $\text{mm}^2$  per  $\text{mm}^2$  of macular area and expressed as a dimensionless percentage. Maximum height was measured in  $\mu\text{m}$ .

A linear mixed effects model ANOVA, taking into account both eyes if appropriate, was computed for each comparison, with the respective metric (normalized volume and area, and maximum height) as the dependent, and the region as the independent variable. Because each patient was measured in each of the regions, and often in both eyes, patient and (nested) eye-specific intercepts were specified. In case of a significant ANOVA, differences between least squares means were computed. However, no control for multiple comparisons between different metrics was performed, because this was an exploratory study. The significance level  $\alpha$  was set to 0.05. To compare the yearly slopes between regions (covered area and normalized volume) the slope for each patient was calculated and the same mixed model ANOVA described above was calculated with the slope as the dependent variable. Each eye was screened for drusen regression defined as a repeated volume decrease of 15% on 2 consecutive visits or a volume reduction of 27.75% on 1 following visit.<sup>42,43</sup> Progression curves were stopped one visit prior to beginning regression.

### Topography of Cone Photoreceptors

Published maps of cone topography in human retinas<sup>12,39</sup> were revisited to estimate the density of cells (cells/ $\text{mm}^2$ ) in ETDRS subfields. These data were originally part of a comprehensive mapping of both cones and rods in flat mounts of short postmortem retinas.<sup>12</sup> The reported cell densities were subsequently validated in vivo by independent studies using adaptive optics scanning laser ophthalmoscopy.<sup>44</sup> Eyes from donors 61 to 90 years of age ( $n = 12$ , 8 men and 4 women, Caucasian, Northwest USA) had macroscopically normal maculae. From the chosen study, cone densities were available at  $x, y$  points in a coordinate system established by centers of the fovea and optic nerve head. These locations were newly projected into a plane using polar coordinates. Delaunay triangulation was used to create images, which were then re-sampled within ETDRS subfields to provide cell densities at precise locations.

### Topography of Macular Pigment

The distribution of macular pigment was assessed by dual wavelength autofluorescence imaging in a population of older adults ( $n = 31$ , mean age =  $75.2 \pm 4.1$  years, 29 Caucasian, 2 African-descent; 20 women; and 1 person reported use of carotenoid-containing oral supplements). All persons had grade 1 (normal) on the Age Related Eye Disease Studies (AREDS) CFP scale for AMD pathology in both eyes.<sup>45</sup> Images were captured with the Spectralis investigational MPOD module, which is a confocal scanning laser ophthalmoscope with blue ( $\lambda_{\text{ex}} = 488 \text{ nm}$ ) and green ( $\lambda_{\text{ex}} = 514 \text{ nm}$ ) laser diodes for autofluorescence excitation. Initial camera alignment, illumination, and focus were done in near-infrared mode. To standardize the screening of excitation light by photopigment, eyes were exposed to a bleaching light for 25 seconds. The camera mode was switched to simultaneous 488 nm (blue) and 514 nm (green) imaging.

**TABLE 1.** Soft Drusen Baseline Characteristics and Growth Rates of Soft Drusen Volume in Area Per Year Including Differences Between Topographic Areas

ETDRS Subfields	Normalized Volumen/ $\text{mm}^2$	Covered Area%	Maximum Height $\mu\text{m}$	Volume Growth Rates $\text{nL}/\text{mm}^2/\text{year}$	Area Growth Rates%/y
Center	$32.9 \pm 41.8$	$43 \pm 31$	$120.5 \pm 54.4$	$9.2 \pm 10.6$	$7.0 \pm 7.3$
Inner ring	$14.4 \pm 16.3$	$24 \pm 20$	$130.9 \pm 51.6$	$3.8 \pm 4.0$	$4.0 \pm 4.4$
Outer ring	$1.7 \pm 2.6$	$4 \pm 5$	$93.6 \pm 39.1$	$0.5 \pm 0.9$	$1.0 \pm 1.4$
Center versus inner ring	$P < 0.001$	$P < 0.001$	$P = 0.084$	$P < 0.001$	$P = 0.009$
Center versus outer ring	$P < 0.001$	$P < 0.001$	$P < 0.001$	$P < 0.001$	$P < 0.001$
Inner versus outer ring	$P = 0.002$	$P < 0.001$	$P < 0.001$	$P = 0.004$	$P < 0.001$
Ratio, center versus outer ring	24.6	10.8	1.3	19.1	7.0
Ratio, center versus inner ring	2.3	1.8	0.9	2.4	1.8
Ratio, inner versus outer rings	10.6	6.0	1.4	8.0	4.0

Soft drusen baseline characteristics and growth rates of normalized soft drusen volume and area per year including differences between topographic areas.

Volume of soft drusen was normalized to nanoliter per square millimeter. Area was calculated as percentage of soft drusen coverage in the respective region and maximum height indicated in micrometer ( $\mu\text{m}$ ). Calculation of growth rate of soft drusen volume indicated in  $\text{nL}/\text{mm}^2$  and area indicated in percentage per year included all data points from follow-up.

Two movies of 140 frames over 30 seconds were captured by flickering the 2 excitation wavelengths, in combination with a barrier filter that blocks all wavelengths  $< 560 \text{ nm}$ . The Spectralis reports correction factors to accommodate a slight mismatch of the excitation wavelengths and macular pigment absorption (approximately  $460 \text{ nm}$ ).<sup>46</sup> MPOD data were exported from the Spectralis and processed by custom FIJI plugins.<sup>47</sup> For each eye, a mean density of MPOD was computed within ETDRS subfields. Means and standard deviations across individuals are reported.

### Topographic Analysis

To compare topographic data across studies, we normalized means of measured parameters (e.g. drusen volume), in three ways. First, mean values in the central subfield and inner ring of the ETDRS grid were divided by mean values in the outer ring. Second, mean values in the central subfield were divided by mean values in the inner ring and then the outer ring, to capture the fall-off with eccentricity from the foveal center. Third, to graphically compare topographies, we normalized values by those in the outer ring.

## RESULTS

### Distribution of Drusen Assessed by OCT Imaging

Sixty-two eyes of 44 Caucasian patients (35 women) with a mean age of  $75.8 \pm 6.85$  years (range = 59.9–92.3 years) and early to intermediate AMD were included in the prospective part of this study. Thirty-seven (59.7%) were right eyes. The mean follow-up time was  $32.7 \pm 17.7$  months, resulting in a total of 494 acquired volume scans. In a total of eight eyes, drusen regression could be observed and were therefore excluded from further analysis.

Table 1 shows that initial mean normalized soft drusen volume was  $32.9 \pm 41.8 \text{ nL}/\text{mm}^2$  for the central subfield,  $14.4 \pm 16.3 \text{ nL}/\text{mm}^2$  for the inner ring, and  $1.7 \pm 2.6 \text{ nL}/\text{mm}^2$  for the outer ring. The percentage of area (footprint) occupied by soft drusen at baseline was  $43 \pm 31\%$  for the central subfield,  $24 \pm 20\%$  for the inner ring, and  $4 \pm 5\%$  for the outer ring. Maximum soft drusen height was  $120.5 \pm 54.4 \mu\text{m}$  for the central disk,  $130.9 \pm 51.6 \mu\text{m}$  for the inner ring, and

$93.6 \pm 39.1 \mu\text{m}$  for the outer ring. Soft drusen load, whether measured in volume or area, differed significantly between each of the three regions (all  $P < 0.001$ , except inner ring – outer ring for volume:  $P = 0.002$ ). Maximum soft drusen height differed significantly between the central disk and the outer ring ( $P < 0.001$ ), as well as between the inner and outer rings ( $P < 0.001$ ), but not between the central disk and the inner ring ( $P = 0.084$ ). Figure 2 summarizes soft drusen metrics, including mean covered area and height.

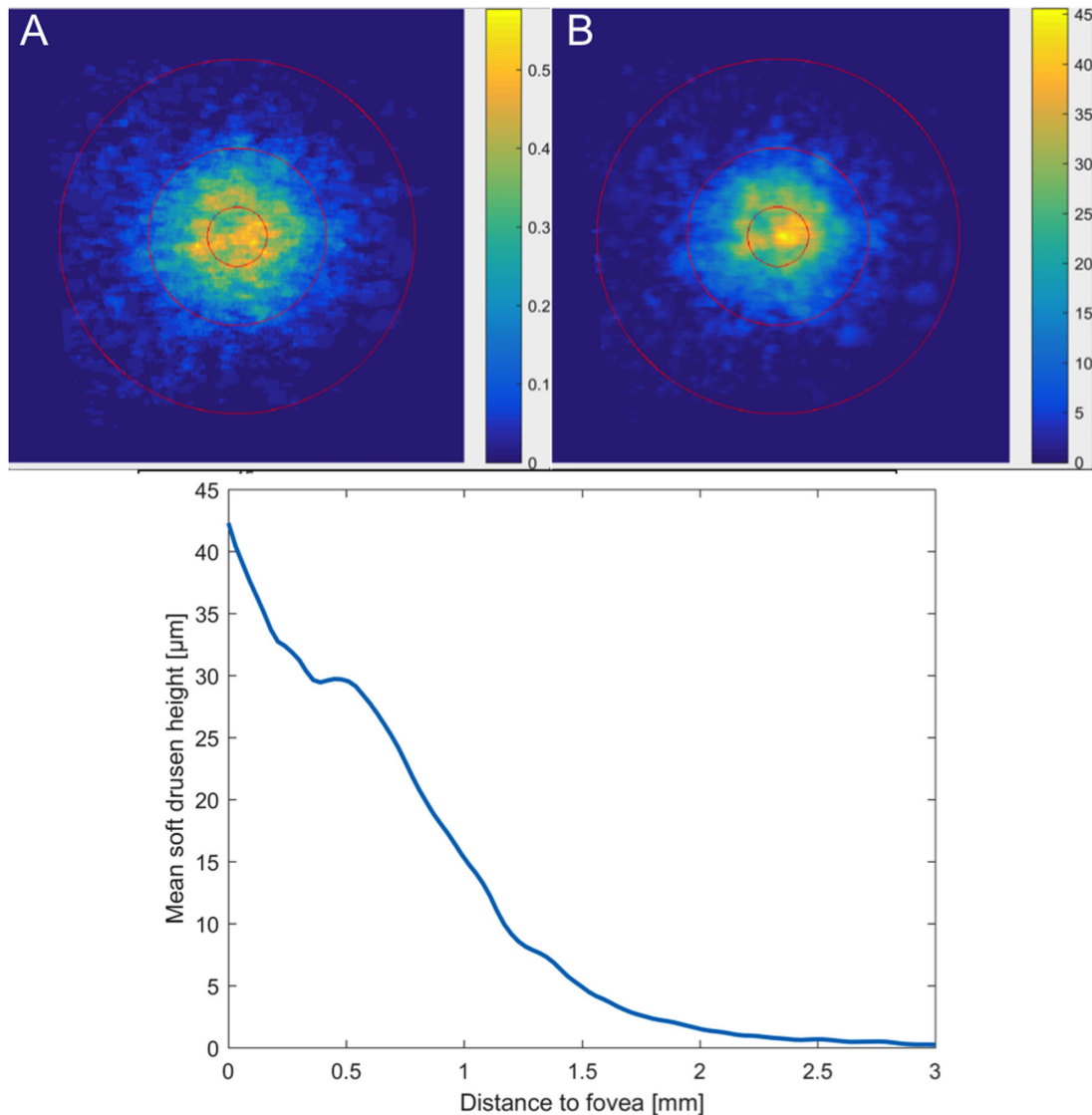
### Differences in Growth Rates

Table 1 shows that growth rates of normalized soft drusen volume increased  $9.17 \pm 10.57 \text{ nL}/\text{mm}^2/\text{year}$  for the central disk,  $3.84 \pm 3.95 \text{ nL}/\text{mm}^2/\text{year}$  for the inner ring, and  $0.48 \pm 0.85 \text{ nL}/\text{mm}^2/\text{year}$  for the outer ring with significant differences between all regions (all  $P < 0.001$ , except inner ring versus the outer ring:  $P = 0.004$ ). Growth in drusen area also revealed significant differences between all regions (all  $P < 0.001$ , except central disk versus inner ring:  $P = 0.009$ ) with  $7 \pm 7.3\%/year$  for the central disk,  $4 \pm 4.4\%/year$  for the inner ring, and  $1 \pm 1.4\%/year$  for the outer ring.

### Comparison of Soft Drusen Topography to Cone Photoreceptors and Macular Pigment

Topographic analysis in Table 1 shows that drusen volume in the central subfield is 24.6-fold higher than in the outer ring and 2.3-fold higher than in the inner ring. The comparable ratios are shown in Table 1 for drusen area (10.8, 1.8), drusen height (1.3, 0.9), drusen volume growth rate (19.1, 2.4), and drusen area growth rates (7.0, 1.8).

In Table 2, we compared OCT-determined soft drusen topography to two tissue-level factors in the neurosensory retina. For the density of cone photoreceptors in eyes of donors 61 to 90 years of age with normal maculae, the central subfield had 13.3-fold higher density than the outer ring and 5.1-fold higher density than the inner ring. For MPOD in the right and left eyes, respectively, of 31 older adults with normal maculae, we found that the central subfield had 24.6 and 23.9-fold higher MPOD than the outer ring, and 3.6 and 3.6-fold higher density than the inner ring (Table 2).



**FIGURE 2.** Soft drusen metrics. **(A)** Spatial distribution of soft drusen across the ETDRS subfields at the baseline visit of eyes with early to intermediate AMD. Each pixel demonstrates the color-coded percentage coverage by soft drusen in that particular location across the baseline visit of analyzed eyes. Soft drusen had a peak accumulation within the central ETDRS subfield with decreasing percentage areas with increasing distance from the foveal center. **(B)** Mean height of soft drusen across the three ETDRS subfields at the baseline visit of eyes with early to intermediate AMD. Each pixel shows the color-coded mean height in  $\mu\text{m}$  of soft drusen present in that specific location. Soft drusen located within the central ETDRS subfield showed the peak height compared to the inner and outer ring. **(C)** Relationship between height of soft drusen and distance from the foveal center. A quantitative topographic profile shows the mean drusen height (in  $\mu\text{m}$ ) of all eyes at the baseline visit, as a function of eccentricity (in mm) computed along circles of increasing diameter starting from the fovea. Soft drusen height falls off sharply with increasing distance from the foveal center.

## DISCUSSION

Our key finding is that the abundance and growth of soft drusen identified by OCT are highly concentrated in the central macula, as they are in CFP. This distribution closely paralleled newly recomputed values for MPOD and less so the density of cone photoreceptors, as published for healthy aged eyes and tissues, respectively. [Figure 3](#) summarizes these findings along with Discussion points that we cover below. We capitalized on advances in OCT imaging to measure volumes of soft drusen based on gold-standard computer-assisted manual assignments. Because of the steep eccentricity gradients of macular cell density associated with acute vision in humans, comparison of topography is a

useful analytic paradigm in human visual neuroscience.<sup>48</sup> We used a standard of retinal localization, the ETDRS grid, to directly compare data on drusen abundance to datasets obtained from different modalities, populations, geographic locations, and epochs of time. Although still in need of additional validation and experimental confirmation, a mechanistic relationship is implied by the similar topographies of soft drusen and MPOD.

The sharp peak and steep gradient that we found for drusen volume was not found for drusen area or height, thus supporting volume as a comprehensive measure of drusen abundance. For the following reasoning, it is more likely that a peak and gradient in any of our metrics is a function of the geometry of participating cells rather than an error

TABLE 2. Comparison of Drusen Volume to Tissue-Level Factors in Neurosensory Retina

ETDRS Subfields*	Normalized Volume nL/mm <sup>2</sup>	Cone/mm <sup>2</sup>	MPOD (OD)	MPOD (OS)
Center	32.9	54,829	0.33	0.35
Inner ring	14.4	10,799	0.09	0.10
Outer ring	1.7	4,125	0.01	0.01
Center/outer	24.6	13.3	24.6	23.9
Center/inner	2.3	5.1	3.6	3.6
Inner/outer	10.6	2.6	6.9	6.6

\* The radii of the ETDRS subfields are 0.5, 1.5, and 3.0 mm. The areas of the ETDRS subfields are 0.79, 6.28, and 21.21 mm<sup>2</sup>. If the central subfield is considered to have unit area, then the area of the inner ring is 8 and the outer ring is 27.

Drusen volume, current data for normalized soft drusen volume, baseline, nL/mm<sup>2</sup>.

Cones,<sup>39</sup> cones/mm<sup>2</sup> in flat-mounted normal retinas, donor age 61 to 90 years.

MPOD (OD, OS), dimensionless macular pigment optical density determined via dual wavelength autofluorescence in 30 older adults with normal maculae. Right and left eyes of the same individuals are shown.

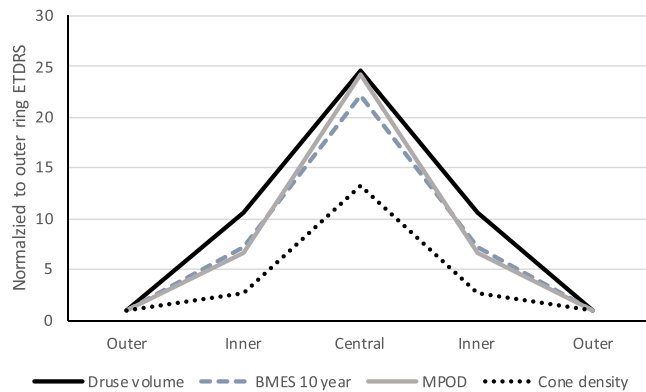


FIGURE 3. Topography of drusen volume, progression risk, and candidate mechanisms. To compare the spatial topography for drusen volume measured in this study to published values for drusen-related progression risk, cone density, and MPOD, all four variables were expressed within ETDRS subfields (central, inner ring, and outer ring) and plotted on the same axis. MPOD for right and left eyes were averaged. Each variable was normalized by its value in the outer ETDRS ring. Values for inner and outer rings are plotted symmetrically on either side of the central subfield. Ratios of the central peak to the outer ring were 22, 25, and 24 for BMES 10-year, drusen volume, and MPOD, respectively, and 13 for cones. The similar topography of drusen volume, progression risk, and MPOD is apparent. Cone density has a lower peak relative to the outer ring and falls off less steeply than the other parameters. BMES, Blue Mountain Eye Study; MPOD, macular pigment optical density.

in measurement technique. The human macula exhibits a foveal singularity with a roughly radially symmetric distribution of cells within eccentricities included in the ETDRS grid. The foveal singularity is particularly narrow for cones and Müller glia in the central bouquet, which is averaged within the central ETDRS subfield.<sup>49</sup> RPE cell density is also maximal in the fovea, but low overall with a very gradual gradient.<sup>50–52</sup> Because of this geometry, imaging techniques (either clinical or laboratory) that are not designed to detect a sharp spike, either due to low resolution or noncomprehensive sampling, will also likely miss the gradient. For example, when adaptive optics made it possible to visualize in vivo the finest foveal cones in a continuous mosaic, it became feasible to statistically compare macular cell distributions across individuals.<sup>12,39,44</sup>

Retinal topography is a strong independent variable linked to evolutionary biology, yet few studies compared

drusen abundance or progression risk across ETDRS subfields. Our study was motivated by findings of extraordinarily high drusen abundance and drusen-related progression risk in ETDRS subfields obtained from CFP, which does not permit volumetric druse measurements, in large population-based observational studies.<sup>5,53</sup> The Beaver Dam Eye Study (BDES) and the Blue Mountain Eye Study (BMES) expressed measures in standardized units that accounted for differences in subfield areas<sup>5,6,53,54</sup> directly comparable with our data (Table 3; Fig. 3). For drusen abundance in the BDES baseline, the central subfield was 7.0-fold higher than the outer ring and 2.8-fold higher than the inner ring.<sup>53</sup> For drusen-related progression risk in the BMES 10-year follow-up, the odds ratio for late AMD by baseline drusen features was 26 for drusen in the central subfield<sup>5</sup> (3.1-fold and 22.1-fold higher than in the inner and outer ring, respectively). In the BMES 15-year follow-up the peak odds ratio (18.5) was lower than at 10 years, which the BMES authors attributed due to disease progression and drop-out of study participants. A similar spatial pattern is visible for drusen volumes recently reported for a clinical trial dataset<sup>55</sup> and normalized for ETDRS subfield area by us in Table 3. Waldstein et al., also using the Iowa Reference Algorithm, determined the volume of all drusen in OCT scans of eyes that stayed stable, progressed to macular atrophy, or progressed to macular neovascularization.<sup>55</sup> For these eyes, drusen volume is maximal in the central subfield; the central-inner-outer gradient (5–7) is markedly shallower than in our study.

By reporting data in the low-risk outer ETDRS ring, studies in Table 3, including ours, highlight the specificity of the high risk central drusen and separate them mechanistically from the numerous other drusen distributed across the fundus. We cannot compare our data directly to other studies reporting drusen abundance within a combined central subfield and inner ring of the ETDRS grid.<sup>54,56</sup> We can compare our data to other studies reporting drusen volume measured with software on another OCT device (Cirrus, Zeiss).<sup>27,57,58</sup> This software calculates total volume under RPE elevations in a 3 mm diameter central circle, equivalent to the ETDRS central subfield plus inner ring. In this area, Yehoshua et al.<sup>27</sup> reported drusen volumes from 0.0009 mm<sup>3</sup> to 0.7479 mm<sup>3</sup>, close to our mean value of 0.1151 mm<sup>3</sup> for soft drusen when converted to comparable units.

A high central drusen load before progression may support a recently articulated model for soft drusen biogenesis and growth. Sarks and associates revealed that the major component of soft drusen is “membranous debris.”<sup>59,60</sup> This

**TABLE 3.** Studies Reporting Concentration of Drusen or Drusen-Related Risk in Central Macula Stratified by ETDRS Grid Subfields, Normalized by Subfield Area

ETDRS Subfields	BDES*	BMES(10-y) <sup>†</sup>	BMES(15-y) <sup>†</sup>	HARBOR-MNV <sup>‡</sup>	HARBOR-MA <sup>‡</sup>	HARBOR-NP <sup>‡</sup>
Center	1.4	26.5	18.5	26.8	19.4	15.3
Inner ring	0.5	8.6	8.2	17.0	11.9	8.9
Outer ring	0.2	1.2	1.4	3.9	3.5	3.1
Center/outer	7.0	22.1	13.2	7.0	5.6	5.0
Center/inner	2.8	3.1	2.3	1.6	1.6	1.7
Inner/outer	2.5	7.2	5.9	4.4	3.4	2.9

\* BDES, Beaver Dam Eye Study, population-based, community-dwelling persons, 43 to 86 years, USA; soft indistinct drusen (% area) at baseline; color fundus photography.<sup>53</sup>

<sup>†</sup> BMES, Blue Mountain Eye Study, population-based, community-dwelling persons,  $\geq 49$  years, Australia; 10- and 15-year incidence of neovascular or atrophic AMD stratified by drusen location at baseline, odds ratios for progression; color fundus photography.<sup>5,6</sup>

<sup>‡</sup> HARBOR, a study of ranibizumab administered monthly or on an as-needed basis in patients with sub-foveal neovascular age-related macular degeneration, fellow eyes to neovascular AMD (nvAMD) in a randomized clinical trial; drusen volume in  $10^6 \text{ mm}^3$  in eyes that progressed to macular neovascularization (MNV), macular atrophy (MA), or non-progressing (NP) as analyzed by Waldstein et al.<sup>55</sup>; OCT with Iowa Reference Algorithm.

component is now thought to represent lipoprotein particles that are constitutively secreted into Bruch's membrane by functional RPE. Transport across the Bruch's membrane-choriocapillaris barrier becomes dysfunctional with aging and AMD due to cross-linking and endothelial cell deterioration and loss. Egress of lipoproteins to the circulation is thus impaired,<sup>61–63</sup> and they build up in Bruch's membrane. BLinD (i.e. a thin layer of soft drusen material continuous with drusen), is thicker under the fovea compared to the perifovea.<sup>15</sup> BLinD may also build up into soft drusen that are then visible on clinical examination. In our study cohort of non-neovascular AMD eyes, the mean gain of soft drusen load was almost 2.5-fold higher in the central 1 mm diameter compared to the inner ETDRS ring and over 25-fold higher than in the outer ring. Drusen volume in the central 1 mm diameter grew almost twice as fast compared to the inner ring and 7 times faster than in the outer ring. This indicates a faster accumulation of membranous debris in areas with highly concentrated foveal cells, which we attribute to a combination of high constitutive lipid traffic and impaired clearance, as elaborated below.

A novel hypothesis posits that this constitutive lipid traffic includes the lifelong delivery of lutein and zeaxanthin to macular cells, leading us to ask whether MPOD in normal older eyes and drusen topography in non-neovascular AMD eyes have similar distributions.<sup>23</sup> The basis of this hypothesis is eightfold. First, lipids isolated from Bruch's membrane are highly enriched in the fatty acid linoleate, which is abundant in diet, and not in docosahexaenoate, which is abundant in neural tissues, especially photoreceptors. Second, of major dietary essentials delivered to the retina, one that is very highly concentrated in the central macula are the xanthophyll carotenoids. Third, recent research in several glio-degenerative diseases indicate that Müller glia in human macula constitutively harbor xanthophyll carotenoid pigments.<sup>64–66</sup> Fourth, Müller glia are sufficiently numerous<sup>21</sup> and elaborate in morphology<sup>67</sup> to account for the carotenoid distribution in the plexiform layers as well as the foveal center, without excluding localization to other cells (e.g. cones). Fifth, Müller glia are sustained by the choroidal<sup>23</sup> as well as the retinal circulation. Sixth, RPE cell lines exhibit receptor-mediated uptake of plasma lipoproteins carrying xanthophylls, and interphotoreceptor retinoid binding protein in subretinal space also binds xanthophylls.<sup>68,69</sup> Seventh, carotenoids are transported in plasma by HDL,<sup>70</sup> and high HDL levels have been associated with

AMD risk.<sup>71</sup> Eighth, sequence variants in HDL genes are the second largest AMD-involved pathway after complement<sup>72</sup>; these genes are expressed by outer retinal cells<sup>15</sup> in addition to hepatocytes and enterocytes.

Strengths of our study include soft drusen determination by human expert readers on B-scans followed by automated full 3D drusen segmentation<sup>32,73</sup> and careful attention to drusen regression so as to find the peak of growth, resulting in comprehensive quantification of drusen volume, height, and area within ETDRS subfields. Additional strengths included comparison to high-quality datasets for the spatial distribution of cones and MPOD under a novel hypothesis linking drusen biology, retinal neuroscience, and a multilayer AMD timeline discerned from eye-tracked OCT imaging. This study also had limitations. The small sample size in the prospective clinical part of this study prevented a meaningful analysis of the effect of race and gender on topography. Soft druse segmentation used an automated image analysis algorithm<sup>32</sup> without manual correction, but good repeatability and reproducibility compared to manual segmentation is generally reported for algorithms.<sup>33,34,74</sup> Axial eye length was not measured in our patients and therefore the lateral scale of the OCT images could not be corrected. Some patients may have already undergone central drusen regression before study inclusion, so generalizability from this patient cohort remains to be determined. Deposits other than soft drusen were not included and should be addressed in future studies to test the specificity of topographic effects. Ideally, drusen volume, cone density, and macular pigment can all be measured in the same genotyped patients; imaging technology to allow such a study now exists and needs to be assembled in one place.

In conclusion, we found using OCT a  $\geq 20$ -fold higher peak of soft drusen volume in the central subfield than in the outer ring. This topography closely paralleled the distribution of macular pigment in an independent set of healthy older eyes. These intraocular factors for progression risk have a larger effect size than others with a strong systemic basis (smoking, odds ratio for progression =  $3^{75}$ ; genetic variants, odds ratio = up to  $6.6^{76}$ ). Our data support volume as a preferred drusen metric for AMD risk assessment and an outcome measure for clinical trials. Our data also support universal tissue-level units of measure such as millimeters and the ETDRS grid as standardized tools for evaluating AMD hypotheses involving retinal physiology and genetics. This effort would be aided by updating the ETDRS

grid to include a smaller central region with high zeaxanthin content,<sup>24</sup> ideally supported with new histologic measurements of the central bouquet, and a larger ring that includes the crest of high rod density and SDD.<sup>12</sup>

### Acknowledgments

C.A. Curcio was supported by National Institutes of Health (NIH) grants R01 R01EY027948 and R01EY029595; institutional support from Research to Prevent Blindness Inc., and EyeSight Foundation of Alabama; Macula Foundation. C. Owsley was supported by the Dorsett Davis Discovery Fund.

Disclosure: **A. Pollreis**, None; **G.S. Reiter**, None; **H. Bogunovic**, None; **L. Baumann**, None; **A. Jakob**, None; **F.G. Schlanitz**, None; **S. Sacu**, None; **C. Owsley**, None; **K.R. Sloan**, None; **C.A. Curcio**, Heidelberg Engineering (F), Genentech/Hoffmann-La Roche (F), MacRegen Inc. (I); **U. Schmidt-Erfurth**, None

### References

1. Flaxman SR, Bourne RRA, Resnikoff S, et al. Global causes of blindness and distance vision impairment 1990-2020: a systematic review and meta-analysis. *Lancet Glob Health*. 2017;5:e1221-e1234.
2. Age-Related Eye Disease Study 2 Research Group. Lutein + zeaxanthin and omega-3 fatty acids for age-related macular degeneration: the Age-Related Eye Disease Study 2 (AREDS2) randomized clinical trial. *JAMA*. 2013;309:2005-2015.
3. Spaide RF, Curcio CA. Drusen characterization with multimodal imaging. *Retina*. 2010;30:1441-1454.
4. Chen L, Messinger JD, Sloan KR, et al. Abundance and multimodal visibility of soft drusen in early age-related macular degeneration: a clinicopathologic correlation. *Retina*. 2020;40:1644-1648.
5. Wang JJ, Rochtchina E, Lee AJ, et al. Ten-year incidence and progression of age-related maculopathy: the Blue Mountains Eye Study. *Ophthalmology*. 2007;114:92-98.
6. Joachim N, Mitchell P, Burlutsky G, Kifley A, Wang JJ. The incidence and progression of age-related macular degeneration over 15 years: the Blue Mountains Eye Study. *Ophthalmology*. 2015;122:2482-2489.
7. Bretillon L, Thuret G, Gregoire S, et al. Lipid and fatty acid profile of the retina, retinal pigment epithelium/choroid, and the lacrimal gland, and associations with adipose tissue fatty acids in human subjects. *Exp Eye Res*. 2008;87:521-528.
8. Wang L, Li CM, Rudolf M, et al. Lipoprotein particles of intraocular origin in human Bruch membrane: an unusual lipid profile. *Invest Ophthalmol Vis Sci*. 2009;50:870-877.
9. Pilgrim MG, Lengyel I, Lanzirotti A, et al. Subretinal pigment epithelial deposition of drusen components including hydroxyapatite in a primary cell culture model. *Invest Ophthalmol Vis Sci*. 2017;58:708-719.
10. Balaratnasingam C, Yannuzzi LA, Curcio CA, et al. Associations between retinal pigment epithelium and drusen volume changes during the lifecycle of large drusenoid pigment epithelial detachments. *Invest Ophthalmol Vis Sci*. 2016;57:5479-5489.
11. Schlanitz FG, Baumann B, Kundi M, et al. Drusen volume development over time and its relevance to the course of age-related macular degeneration. *Br J Ophthalmol*. 2017;101:198-203.
12. Curcio CA, Sloan KR, Kalina RE, Hendrickson AE. Human photoreceptor topography. *J Comp Neurol*. 1990;292:497-523.
13. Steinberg JS, Gobel AP, Fleckenstein M, Holz FG, Schmitz-Valckenberg S. Reticular drusen in eyes with high-risk characteristics for progression to late-stage age-related macular degeneration. *Br J Ophthalmol*. 2015;99:1289-1294.
14. Zarubina AV, Neely DC, Clark ME, et al. Prevalence of subretinal drusenoid deposits in older persons with and without age-related macular degeneration, by multimodal imaging. *Ophthalmology*. 2016;123:1090-1100.
15. Curcio CA, Messinger JD, Sloan KR, McGwin G, Medeiros NE, Spaide RF. Subretinal drusenoid deposits in non-neovascular age-related macular degeneration: morphology, prevalence, topography, and biogenesis model. *Retina*. 2013;33:265-276.
16. Reiter GS, Told R, Schranz M, et al. Subretinal drusenoid deposits and photoreceptor loss detecting global and local progression of geographic atrophy by SD-OCT imaging. *Invest Ophthalmol Vis Sci*. 2020;61:11.
17. Molday RS, Moritz OL. Photoreceptors at a glance. *J Cell Sci*. 2015;128:4039-4045.
18. Arshavsky VY, Burns ME. Photoreceptor signaling: supporting vision across a wide range of light intensities. *J Biol Chem*. 2012;287:1620-1626.
19. Thoreson WB, Dacey DM. Diverse cell types, circuits, and mechanisms for color vision in the vertebrate retina. *Physiol Rev*. 2019;99:1527-1573.
20. Quinn N, Csincsik L, Flynn E, et al. The clinical relevance of visualising the peripheral retina. *Prog Retin Eye Res*. 2019;68:83-109.
21. Ahmad KM, Klug K, Herr S, Sterling P, Schein S. Cell density ratios in a foveal patch in macaque retina. *Vis Neurosci*. 2003;20:189-209.
22. Syrbe S, Kuhrt H, Gartner U, et al. Muller glial cells of the primate foveola: an electron microscopical study. *Exp Eye Res*. 2018;167:110-117.
23. Curcio CA. Antecedents of soft drusen, the specific deposits of age-related macular degeneration, in the biology of human macula. *Invest Ophthalmol Vis Sci*. 2018;59:AMD182-AMD194.
24. Li B, George EW, Rognon GT, et al. Imaging lutein and zeaxanthin in the human retina with confocal resonance Raman microscopy. *Proc Natl Acad Sci USA*. 2020;117:12352-12358.
25. Snodderly DM, Auran JD, Delori FC. The macular pigment. II. Spatial distribution in primate retinas. *Invest Ophthalmol Vis Sci*. 1984;25:674-685.
26. Asgari R, Orlando JI, Waldstein S, et al. Multiclass segmentation as multitask learning for drusen segmentation in retinal optical coherence tomography. *Med Image Comput Comput Assist Interv*. 2019;11764:192-200.
27. Yehoshua Z, Wang F, Rosenfeld PJ, Penha FM, Feuer WJ, Gregori G. Natural history of drusen morphology in age-related macular degeneration using spectral domain optical coherence tomography. *Ophthalmology*. 2011;118:2434-2441.
28. de Sistiernes L, Simon N, Tibshirani R, Leng T, Rubin DL. Quantitative SD-OCT imaging biomarkers as indicators of age-related macular degeneration progression. *Invest Ophthalmol Vis Sci*. 2014;55:7093-7103.
29. de Sistiernes L, Jonna G, Moss J, Marmor MF, Leng T, Rubin DL. Automated intraretinal segmentation of SD-OCT images in normal and age-related macular degeneration eyes. *Biomed Opt Express*. 2017;8:1926-1949.
30. Chen Q, Leng T, Zheng L, et al. Automated drusen segmentation and quantification in SD-OCT images. *Med Image Anal*. 2013;17:1058-1072.
31. Yang Q, Reisman Ca, Wang Z, et al. Automated layer segmentation of macular OCT images using dual-scale gradient information. *Opt Express*. 2010;18:21293-21307.

32. Bogunovic H, Montuoro A, Baratsits M, et al. Machine learning of the progression of intermediate age-related macular degeneration based on OCT imaging. *Invest Ophthalmol Vis Sci.* 2017;58:141–150.
33. Freeman SR, Kozak I, Cheng L, et al. Optical coherence tomography-raster scanning and manual segmentation in determining drusen volume in age-related macular degeneration. *Retina.* 2010;30:431–435.
34. Nittala MG, Ruiz-Garcia H, Sadda SR. Accuracy and reproducibility of automated drusen segmentation in eyes with non-neovascular age-related macular degeneration. *Invest Ophthalmol Vis Sci.* 2012;53:8319–8324.
35. Khanifar AA, Koreishi AF, Izatt JA, Toth CA. Drusen ultrastructure imaging with spectral domain optical coherence tomography in age-related macular degeneration. *Ophthalmology.* 2008;115:1883–1890.
36. Rudolf M, Clark ME, Chimento MF, Li CM, Medeiros NE, Curcio CA. Prevalence and morphology of druse types in the macula and periphery of eyes with age-related maculopathy. *Invest Ophthalmol Vis Sci.* 2008;49:1200–1209.
37. Balaratnasingam C, Cherepanoff S, Dolz-Marco R, et al. Cuticular drusen: clinical phenotypes and natural history defined using multimodal imaging. *Ophthalmology.* 2018;125:100–118.
38. Freund KB, Laud K, Lima LH, Spaide RF, Zweifel S, Yannuzzi LA. Acquired vitelliform lesions: correlation of clinical findings and multiple imaging analyses. *Retina.* 2011;31:13–25.
39. Curcio CA, Millican CL, Allen KA, Kalina RE. Aging of the human photoreceptor mosaic: evidence for selective vulnerability of rods in central retina. *Invest Ophthalmol Vis Sci.* 1993;34:3278–3296.
40. Garrity ST, Sarraf D, Freund KB, Sadda SR. Multimodal imaging of nonneovascular age-related macular degeneration. *Invest Ophthalmol Vis Sci.* 2018;59:AMD48.
41. Early Treatment Diabetic Retinopathy Study Research Group. Grading diabetic retinopathy from stereoscopic color fundus photographs—an extension of the modified Airlie House classification. ETDRS report number 10. *Ophthalmology.* 1991;98:786–806.
42. Baumann B, Gotzinger E, Pircher M, et al. Segmentation and quantification of retinal lesions in age-related macular degeneration using polarization-sensitive optical coherence tomography. *J Biomed Opt.* 2010;15:061704.
43. Schlanitz FG, Baumann B, Kundi M, et al. Drusen volume development over time and its relevance to the course of age-related macular degeneration. *Br J Ophthalmol.* 2017;101:198–203.
44. Zhang T, Godara P, Blanco ER, et al. Variability in human cone topography assessed by adaptive optics scanning laser ophthalmoscopy. *Am J Ophthalmol.* 2015;160:290–300.e291.
45. Davis MD, Gangnon RE, Lee LY, et al. The Age-Related Eye Disease Study severity scale for age-related macular degeneration: AREDS Report No. 17. *Arch Ophthalmol.* 2005;11:1484–1498.
46. Conrady CD, Bell JP, Besch BM, et al. Correlations between macular, skin, and serum carotenoids. *Invest Ophthalmol Vis Sci.* 2017;58:3616–3627.
47. Schindelin J, Arganda-Carreras I, Frise E, et al. Fiji: an open-source platform for biological-image analysis. *Nat Methods.* 2012;7:676–682.
48. Wassle H, Boycott BB. Functional architecture of the mammalian retina. *Physiol Rev.* 1991;71:447–480.
49. Govetto A, Bhavsar KV, Virgili G, et al. Tractional abnormalities of the central foveal bouquet in epiretinal membranes: clinical spectrum and pathophysiological perspectives. *Am J Ophthalmol.* 2017;184:167–180.
50. Gao H, Hollyfield JG. Aging of the human retina. Differential loss of neurons and retinal pigment epithelial cells. *Invest Ophthalmol Vis Sci.* 1992;33:1–17.
51. Snodderly DM, Sandstrom MM, Leung IY, Zucker CL, Neuringer M. Retinal pigment epithelial cell distribution in central retina of rhesus monkeys. *Invest Ophthalmol Vis Sci.* 2002;43:2815–2818.
52. Ach T, Huisinigh C, McGwin G, Jr, et al. Quantitative autofluorescence and cell density maps of the human retinal pigment epithelium. *Invest Ophthalmol Vis Sci.* 2014;55:4832–4841.
53. Wang Q, Chappell RJ, Klein R, et al. Pattern of age-related maculopathy in the macular area. The Beaver Dam Eye Study. *Invest Ophthalmol Vis Sci.* 1996;37:2234–2242.
54. Joachim ND, Mitchell P, Kifley A, Wang JJ. Incidence, progression, and associated risk factors of medium drusen in age-related macular degeneration: findings from the 15-year follow-up of an Australian cohort. *JAMA Ophthalmol.* 2015;133:698–705.
55. Waldstein SM, Vogl WD, Bogunovic H, Sadeghipour A, Riedl S, Schmidt-Erfurth U. Characterization of drusen and hyperreflective foci as biomarkers for disease progression in age-related macular degeneration using artificial intelligence in optical coherence tomography. *JAMA Ophthalmol.* 2020;138:740–747.
56. Chew EY, Clemons TE, Agron E, et al. Ten-year follow-up of age-related macular degeneration in the age-related eye disease study: AREDS report no. 36. *JAMA Ophthalmol.* 2014;132:272–277.
57. Diniz B, Rodger DC, Chavali VR, et al. Drusen and RPE atrophy automated quantification by optical coherence tomography in an elderly population. *Eye.* 2015;29:272–279.
58. Chavali VR, Diniz B, Huang J, Ying GS, Sadda SR, Stambolian D. Association of OCT derived drusen measurements with AMD associated-genotypic SNPs in Amish population. *J Clin Med.* 2015;4:304–317.
59. Sarks JP, Sarks SH, Killingsworth MC. Evolution of geographic atrophy of the retinal pigment epithelium. *Eye.* 1988;2:552–577.
60. Sarks JP, Sarks SH, Killingsworth MC. Evolution of soft drusen in age-related macular degeneration. *Eye.* 1994;8:269–283.
61. Malek G, Li C-M, Guidry C, Medeiros NE, Curcio CA. Apolipoprotein B in cholesterol-containing drusen and basal deposits of human eyes with age-related maculopathy. *Am J Pathol.* 2003;162:413–425.
62. Anderson DH, Ozaki S, Nealon M, et al. Local cellular sources of apolipoprotein E in the human retina and retinal pigmented epithelium: implications for the process of drusen formation. *Am J Ophthalmol.* 2001;131:767–781.
63. Mullins RF, Russell SR, Anderson DH, Hageman GS. Drusen associated with aging and age-related macular degeneration contain proteins common to extracellular deposits associated with atherosclerosis, elastosis, amyloidosis, and dense deposit disease. *FASEB J.* 2000;14:835–846.
64. Charbel Issa P, Gillies MC, Chew EY, et al. Macular telangiectasia type 2. *Prog Retin Eye Res.* 2013;34:49–77.
65. Pang CE, Maberley DA, Freund KB, et al. Lamellar hole-associated epiretinal proliferation: a clinicopathologic correlation. *Retina.* 2016;36:1408–1412.
66. Nanda T, Kovach JL. Ophthalmic findings in late stage Sjogren-Larsson syndrome. *Retin Cases Brief Rep.* 2019;13:251–254.
67. Bringmann A, Syrbe S, Gorner K, et al. The primate fovea: structure, function and development. *Prog Retin Eye Res.* 2018;66:49–84.

68. Thomas SE, Harrison EH. Mechanisms of selective delivery of xanthophylls to retinal pigment epithelial cells by human lipoproteins. *J Lipid Res.* 2016;57:1865–1878.
69. Vachali PP, Besch BM, Gonzalez-Fernandez F, Bernstein PS. Carotenoids as possible interphotoreceptor retinoid-binding protein (IRBP) ligands: a surface plasmon resonance (SPR) based study. *Arch Biochem Biophys.* 2013;539:181–186.
70. Loane E, Nolan JM, O'Donovan O, Bhosale P, Bernstein PS, Beatty S. Transport and retinal capture of lutein and zeaxanthin with reference to age-related macular degeneration. *Surv Ophthalmol.* 2008;53:68–81.
71. Colijn JM, den Hollander AI, Demirkan A, et al. Increased high-density lipoprotein levels associated with age-related macular degeneration: evidence from the EYE-RISK and European Eye Epidemiology Consortia. *Ophthalmology.* 2019;126:393–406.
72. Fritsche LG, Igl W, Bailey JN, et al. A large genome-wide association study of age-related macular degeneration highlights contributions of rare and common variants. *Nat Genet.* 2016;48:134–143.
73. Garvin MK, Abramoff MD, Kardon R, Russell SR, Wu X, Sonka M. Intraretinal layer segmentation of macular optical coherence tomography images using optimal 3-D graph search. *IEEE Trans Med Imag.* 2008;27:1495–1505.
74. de Sisternes L, Jonna G, Greven MA, Chen Q, Leng T, Rubin DL. Individual drusen segmentation and repeatability and reproducibility of their automated quantification in optical coherence tomography images. *Transl Vis Sci Technol.* 2017;6:12.
75. Smith W, Assink J, Klein R, et al. Risk factors for age-related macular degeneration: pooled findings from three continents. *Ophthalmology.* 2001;108:697–704.
76. de Breuk A, Acar IE, Kersten E, et al. Development of a genotype assay for age-related macular degeneration: the EYE-RISK Consortium. *Ophthalmology*, <https://doi.org/10.1016/j.ophtha.2020.07.037>.